Figures and figure supplements

Ciliary chemosensitivity is enhanced by cilium geometry and motility

David Hickey *et al*

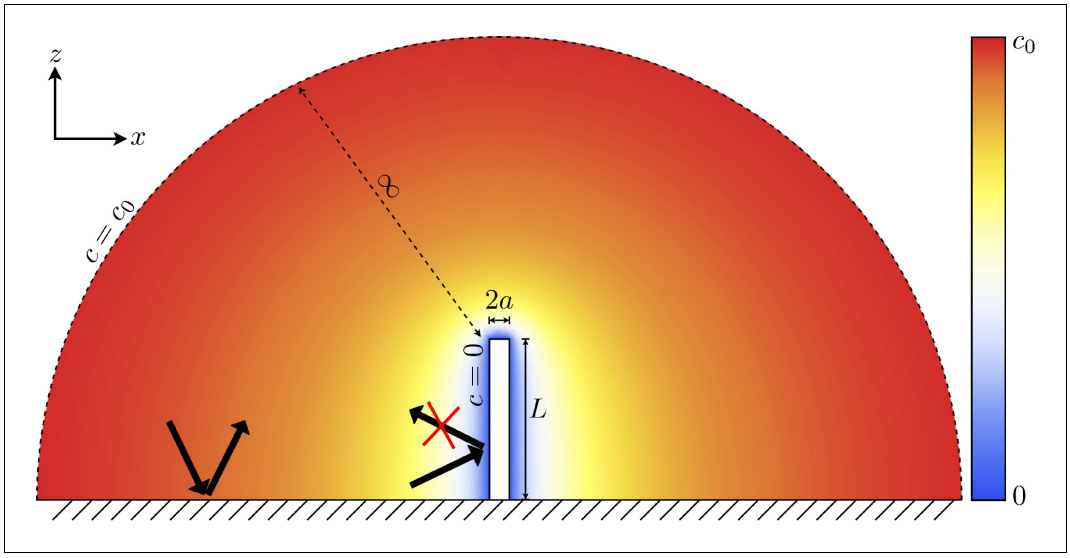

Figure 1. The concentration boundary conditions and general setup of the problem to be solved. The cilium satisfies an absorbing boundary condition, and there is a constant concentration an infinite distance from the cilium. The coloured overlay shows the concentration field in the absence of any fluid flow.

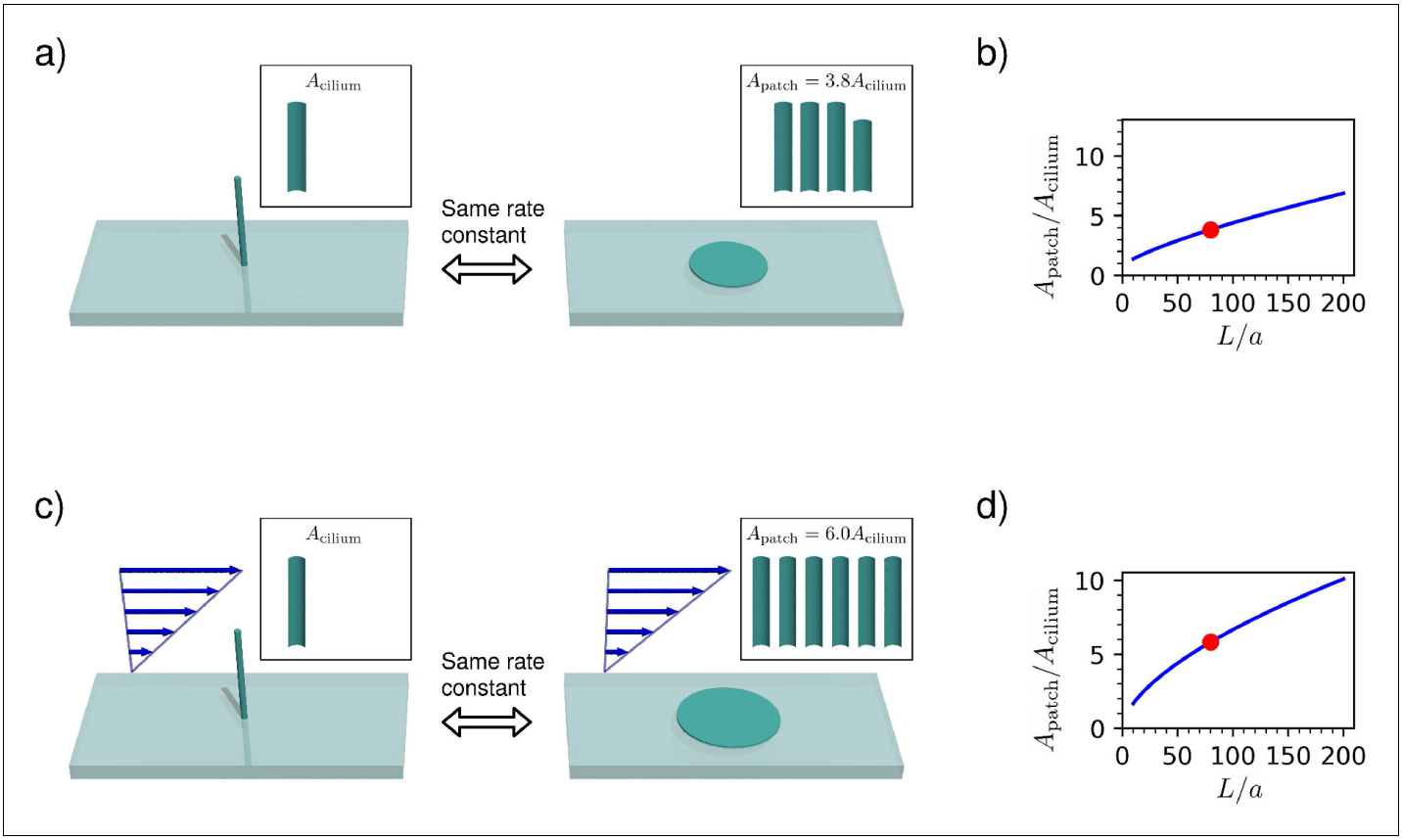

Figure 2. Comparison between capture rates of a non-motile cilium and a circular patch on the surface. All diagrams use $L/a = 80$, indicated on the graphs by a red dot. (**a**) In a quiescent fluid, the cilium has the same capture rate as a surface patch with 3.8 times the surface area. (**b**) The area ratio $A_{\text{patch}}/A_{\text{cilium}}$ as a function of the cilium aspect ratio L/a in a quiescent fluid, given by ***Equation (6)***. (**c**) In a shear flow at a high Péclet number, the capture rate of the cilium reaches that of a surface patch with 6.0 times the surface area. (**d**) The area ratio as a function of the aspect ratio in the high Péclet number limit (***Equation 14***).

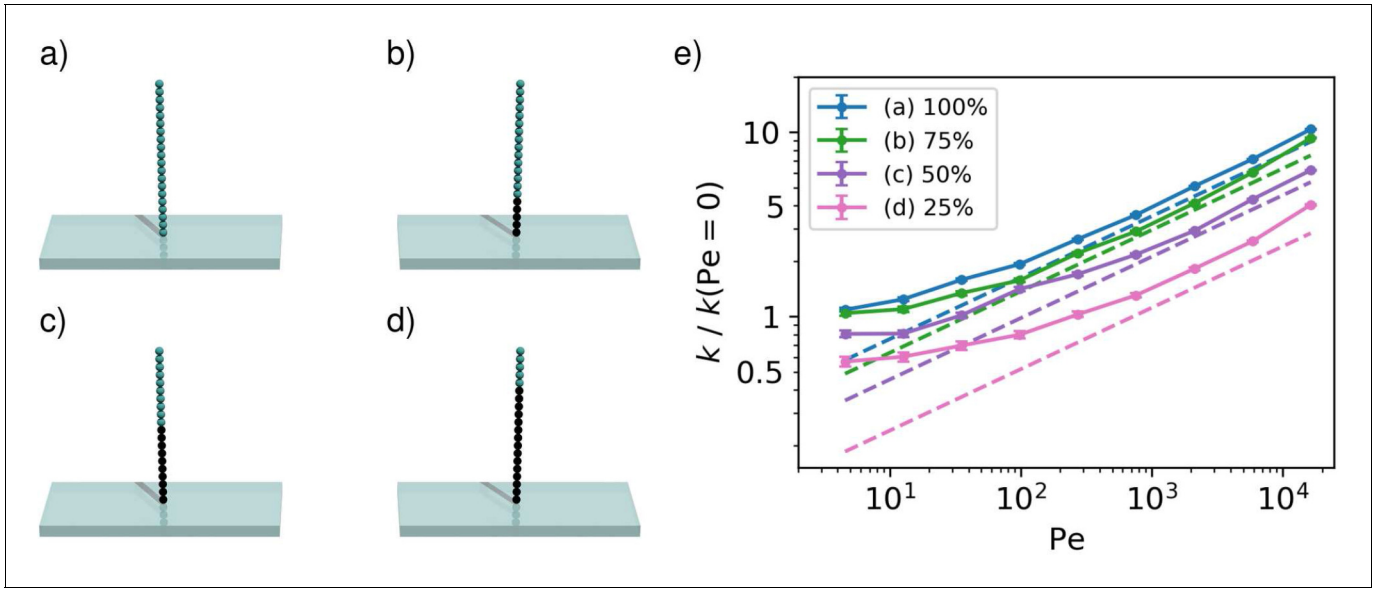

Figure 2—figure supplement 1. Capture rate as a function of the Péclet number for passive cilia in a shear flow, obtained from numerical simulations. The lines show the capture rates for cilia that absorb particles only on a fraction of their length, starting from the tip. The schematics indicate the absorbing part of the cilium in blue and the non-absorbing part in black.

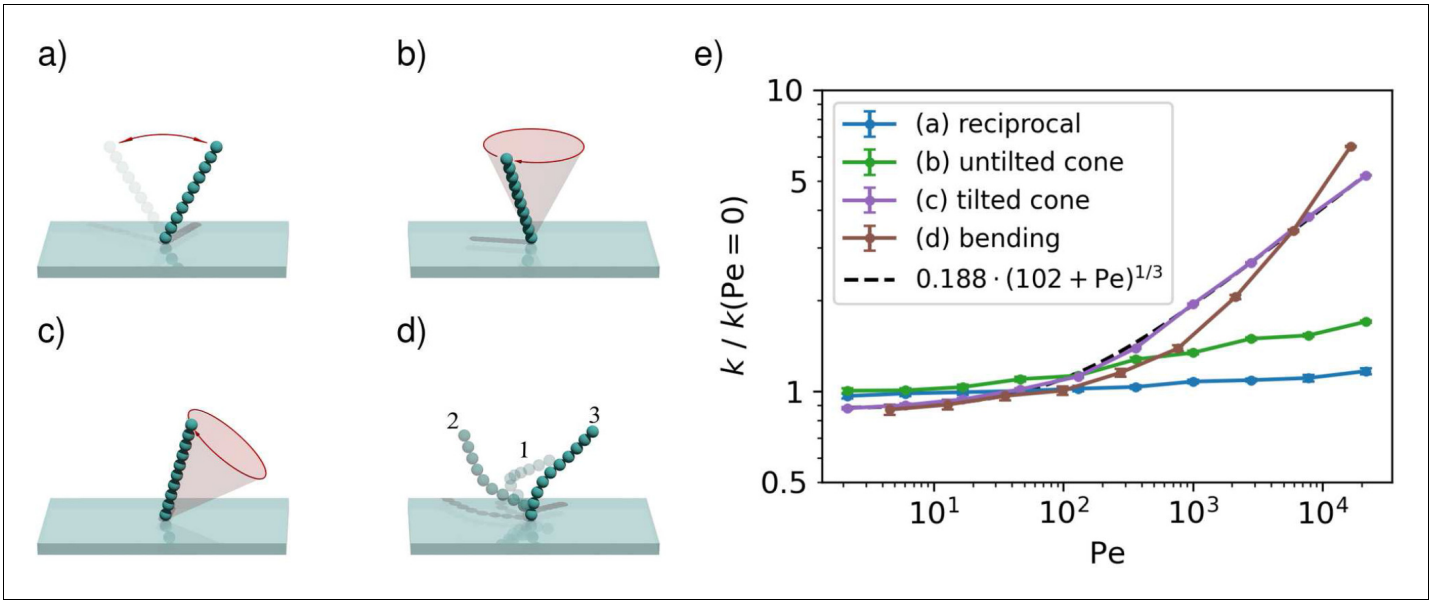

Figure 3. The capture rate of an active cilium for four types of motion. (**a**) The cilium is undergoing reciprocal motion, which is not generating any net flow. (**b**) The cilium moves along a cone with its axis perpendicular to the surface, such that it produces a rotational flow, but no long-range fluid transport. (**c**) The cilium moves along a tilted cone, which generates a long-range volume flow. (**d**) The cilium follows a realistic trajectory, beginning with a recovery stroke along the no-slip surface in 1, then performing an overhead power-stroke from 2 to 3 before returning to one in another recovery stroke. (**e**) The capture rate constants k of a beating cilium as a function of the Péclet number. The rates are determined using stochastic simulations. The error bars denote 95% confidence intervals and the dashed line shows a fit function that interpolates between the high and low-Péclet limits. All rates are normalised to the rate constant for a diffusion-limited capture with a cylindrical cilium with the same length and width.

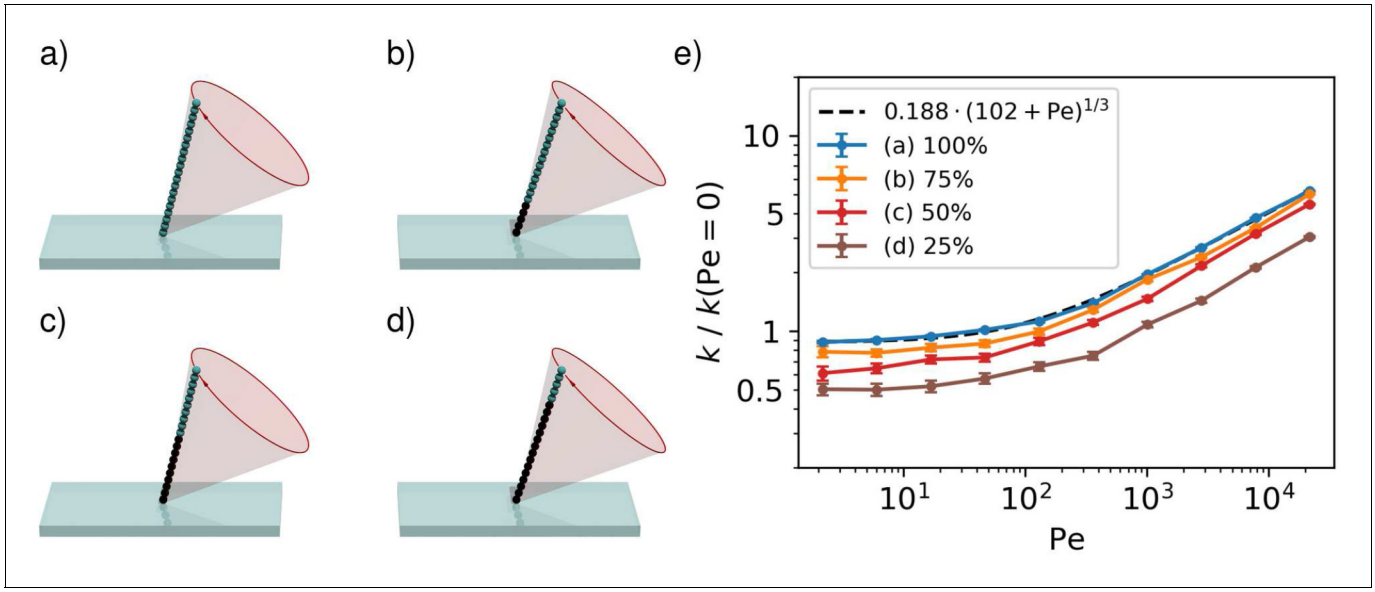

Figure 3—figure supplement 1. Capture rate of an actively beating cilium tracing out a tilted cone, plotted as a function of the Péclet number. These results were obtained from numerical simulations. The lines show the capture rates for cilia that absorb particles only on a fraction of their length, starting from the tip. The schematics indicate the absorbing part of the cilium in blue and the non-absorbing part in black.

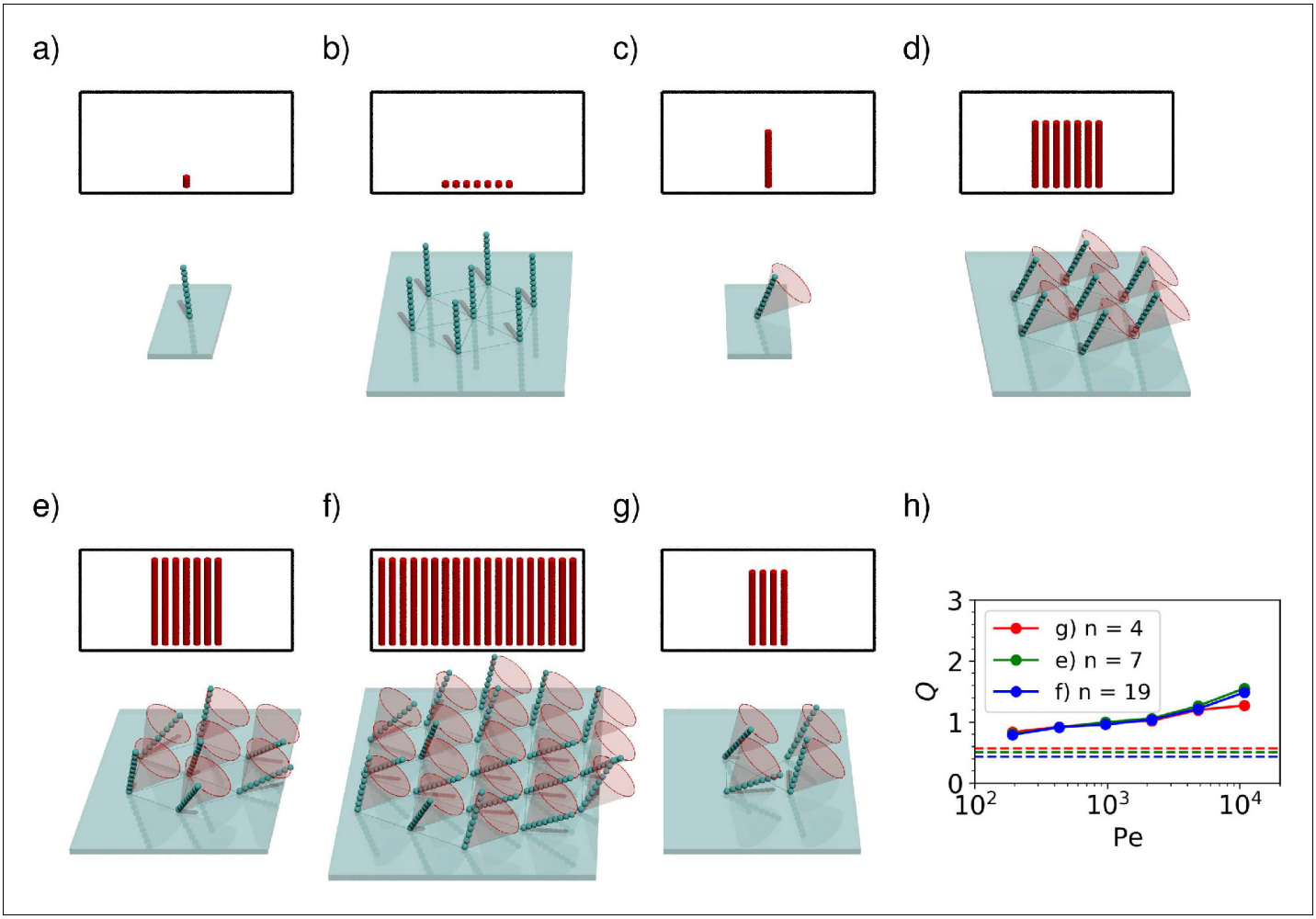

Figure 4. Comparison between the capture rate constant of a single cilium (**a, c**) and a bundle of $N_{\text{cilia}} \in \{4, 7, 19\}$ cilia (**b, d–g**). In the insets, the height of each red cylinder indicates the rate constant per cilium at $\text{Pe} \approx 10000$, and the number of cylinders represents the number of cilia. For immotile cilia (**a, b**), a bundle has a lower per-cilium capture rate than an isolated cilium, although the the total rate constant of the bundle is higher. The reduced capture rate per cilium is caused by the depletion of ligands close to the bundle. For motile cilia (**d–g**), the situation is reversed and the capture rate per cilium in a bundle (**d–g**) can be significantly higher than for an isolated cilium (**c**). The increase can be explained by the collective flow generation, which helps the capture on all cilia. In (**d**) the cilia all beat with the same frequency corresponding to $\text{Pe} \approx 10000$ but with identical phases. In (**e–g**) all cilia beat with the same frequency corresponding to $\text{Pe} \approx 10000$, but their phases are chosen randomly. It can be seen that the random phases give a higher rate constant than the uniform phases. (**h**) shows how the performance gain Q varies with the Péclet number for different configurations. The rates shown at each point are the average of 30 random phase configurations like the one shown in (**e**). The dashed line is the Q-value for $\text{Pe} = 0$ for each configuration.

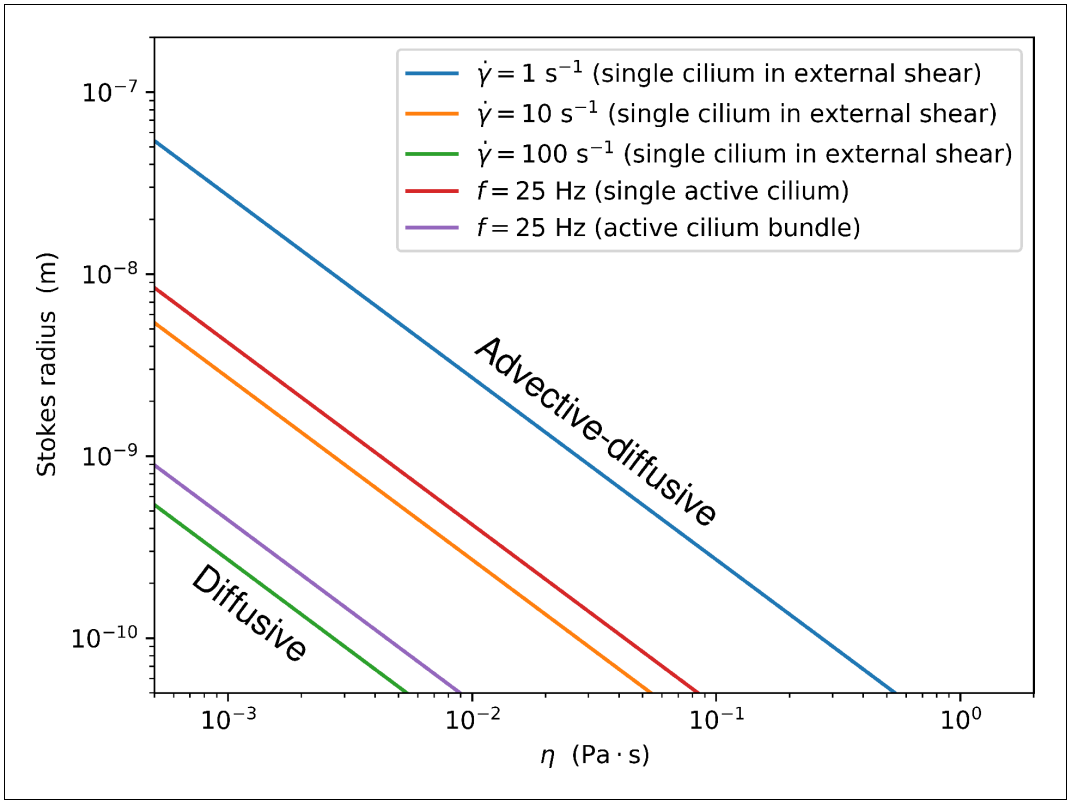

Figure 5. The demarcation between the regime where the rate constant is determined mostly by the diffusion limit and the regime in which it is enhanced by advection as a function of the fluid viscosity η and the particle Stokes radius. The blue, orange, and green lines show the results for a passive cilium in a shear flow (***Figure 2c***), the red line for an actively beatig cilium (***Figure 3c***) and the magenta line for a bundle of 7 cilia (***Figure 4e***). For all lines, the cilium dimensions are $L = 10\,\mu\mathrm{m}$ and $a = 250\,\mathrm{nm}$.

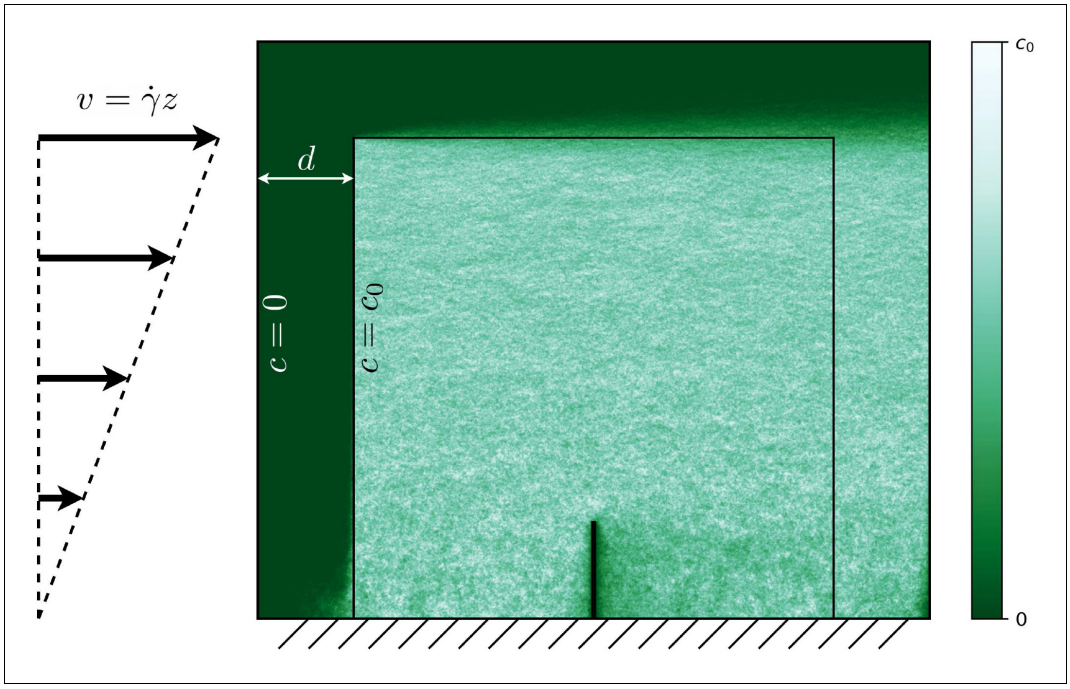

Figure 6. The boundary conditions used for injection. Since the fraction in incident particles absorbed by the cilium is small compared to the fraction absorbed by the outer surface, the concentration at the inner boundary is very close to c_0. The coloured overlay shows the concentration as recorded in an example numerical simulation of a cilium in a shear flow with $\mathrm{Pe} = 50$.

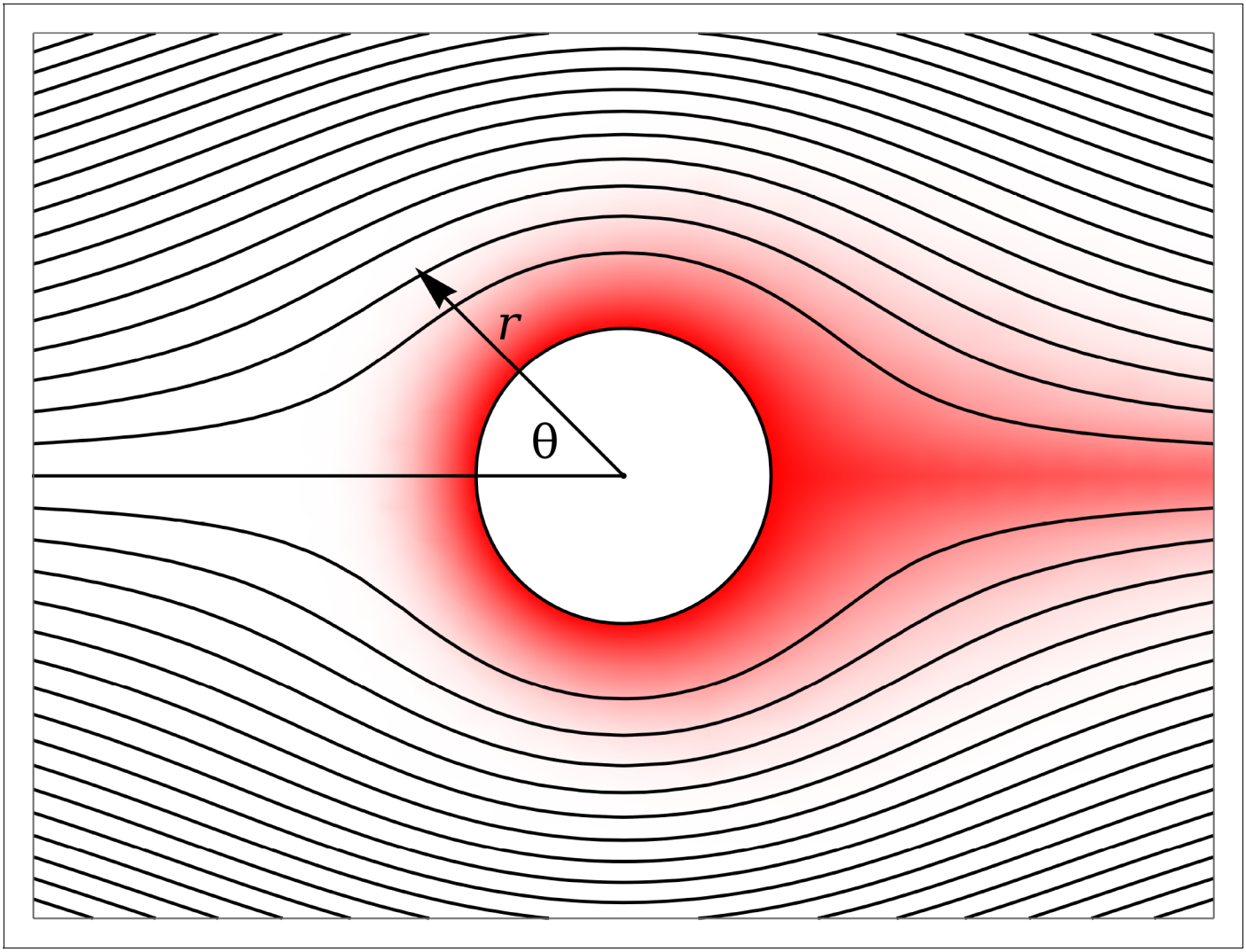

Appendix 2—figure 1. Streamlines (lines with a constant value of the stream function ψ) of the flow around a cylinder (black) and the concentration c of emitted particles (red).